IEEE Access
Multidisciplinary ⋮ Rapid Review ⋮ Open Access Journal

Received 1 February 2024, accepted 23 February 2024, date of publication 26 February 2024, date of current version 7 March 2024.

Digital Object Identifier 10.1109/ACCESS.2024.3370430

RESEARCH ARTICLE

Classical Coherent States Based Quantum Information Processing and Quantum Computing Analogs

IVAN B. DJORDJEVIC, (Fellow, IEEE), AND VIJAY NAFRIA
Department of Electrical and Computer Engineering, University of Arizona, Tucson, AZ 85721, USA

Corresponding author: Ivan B. Djordjevic (ivan@arizona.edu)

The paper was supported in part by the Science and Technology Center New Frontiers of Sound through National Science Foundation Grant No. 2242925 and NSF under Grant 2244365.

ABSTRACT It has been recently demonstrated by Bellini's group that macroscopic states, such as coherent states, can be entangled by the delocalized photon addition. Deymier's group has shown that phase bits (phi-bits) gates implemented by employing the topological acoustics (TA) principles can be used to implement the TA-based quantum computing analogs. This motivates us to revisit our previous papers where we have already described how to implement the universal quantum gates in integrated optics using optical hybrid, directional coupler, Mach-Zehnder interferometer, and periodically poled lithium niobate (PPLN) waveguides, but in a different context. In this paper, we describe how to implement the universal set of quantum gates classical analogs in integrated optics by employing classical polarization states derived from classical coherent states. The main problem for integrated optics implementation on a single photon level has been to implement the controlled-phase gate because the existing optical nonlinear devices where incapable of introducing the π rad phase shift on a single photon level through the Kerr effect, which is not a problem at all when the classical polarization states are used instead. We also describe how to implement quantum qudit analogs based on orbital angular momentum (OAM) states and corresponding qudit gates. To highlight the importance of the proposed concepts, we experimentally demonstrate the controlled-phase gate analog operation between the classical coherent states.

INDEX TERMS Entanglement, coherent states, polarization states, orbital angular momentum (OAM) states, quantum computing, integrated optics, optical quantum computing analogs.

I. INTRODUCTION

The quantum information processing (QIP) [1], [2], [3], [4], [5], [6], [7], [8], [9], [10], [11], [12], [13], [14], [15], [16], [17], [18], [19], [20], [21], [22], [23], [24], [25] is a very active research area with large number of applications including quantum computing [5], [6], [7], [8], [9], [10], [11], [12], [13], [14], [15], [16], [17], [18], [19], quantum communications [20], [21], [22], [23], quantum networks [23], [24], [25], and quantum sensing [23], [26], to mention few. Further, significant efforts have been made towards the commercialization of quantum computers [27], [28], [29]. Moreover, numerous quantum computing libraries have been developed such as Qiskit, Cirq, Forest, ProjectQ, and Quantum development kit (QDK) [17], [30], [31]. Typically, the following three features of QIP are considered different from classical computing [5], [10], [20], [24]: linear superposition, entanglement, and quantum parallelism. The linear superposition indicates that the qubit is represented as a linear combination of the basis states, while in classical computing only two discrete bits (0 and 1) are used. On the other hand, superposition principle is a basic principle applicable to any linear system, not necessarily quantum. Even though state-of-the-art digital computers indeed use just 0 and 1 bits to store information to compute, the future classical computers do not need to be binary only. The entangled states are particular quantum states that cannot be decomposed into independent quantum states. However, recently Bellini's group have demonstrated

The associate editor coordinating the review of this manuscript and approving it for publication was Stanley Cheung.

© 2024 The Authors. This work is licensed under a Creative Commons Attribution-NonCommercial-NoDerivatives 4.0 License.
For more information, see https://creativecommons.org/licenses/by-nc-nd/4.0/

experimentally that macroscopic states, including coherent states, can be entangled by the delocalized photon addition [1]. Quantum parallelism is the capability to parallelly conduct a large number of operations. Recently, Deymier's group have shown that the quantum algorithms can be run on topological acoustic (TA)-based quantum analogs, which are essentially classical computers, and that the nonlinearity is a key enabler for so called quantum parallelism [2], [3], [4]. These recent findings have motivated us to revisit our previous QIP proposals for integrated optics implementations [11], [12], [13], [14], [15], [16], [17], [18], [19], but now in the context of optical quantum computing analogs.

In this paper, we propose how to implement classical optical quantum computing analogs in integrated optics by employing the coherent states as the qubit analogs. We experimentally demonstrate the controlled-phase operation between the classical coherent states. We also describe the qudit classical analogs and corresponding gates based on the orbital angular momentum (OAM) states.

The organization of the paper is summarized in the rest of this section. The classical polarization states and the action on them by the polarizing elements, characterized by using the Jones formalism, is described in Sec. II. In the same section, we explain how to entangle coherent states based on [1] and [25]. In Sec. III, we describe classical single-qubit analogs' implementations in integrated optics by employing the optical hybrid, directional coupler, and Mach-Zehnder interferometer. In Sec. IV, we describe how to implement classical two-qubit analogs in integrated optics, namely controlled-phase and CNOT gate analogs. We also describe how to implement the generic classical Bell state preparation circuit and quantum relay analogs. To illustrate the high-potential of the proposed integrated optics-based classical quantum computing analog concepts, we perform the experimental demonstration of the controlled-phase operation. In Sec. V, we describe the classical quantum qudit equivalent based on OAM and introduce single-qudit and two-qudit gates analogs' implementations in integrated optics.

II. CLASSICAL POLARIZATION STATES AND ENTANGLEMENT OF CLASSICAL STATES

The Jones representation of the polarized light is given by [17], [32]:

$$E = \begin{bmatrix} E_H \\ E_V \end{bmatrix} = \begin{bmatrix} E_{H0}e^{j\phi_H} \\ E_{V0}e^{j\phi_V} \end{bmatrix}, \tag{1}$$

where $E_{H0}(E_{V0})$ is the amplitude in the horizontal (vertical) polarization state and $\phi_H(\phi_V)$ is the corresponding phase. The intensity I can be determined by

$$I = \boldsymbol{E}^{\dagger}\boldsymbol{E} = \begin{bmatrix} E_{H0}^* & E_{V0}^* \end{bmatrix} \begin{bmatrix} E_{H0} \\ E_{V0} \end{bmatrix} = |E_{H0}|^2 + |E_{V0}|^2, \tag{2}$$

and if we normalize it to 1, we can use the Dirac notation [33], [34] to represent arbitrary classical polarization states:

$$|\psi\rangle = \begin{bmatrix} \psi_H \\ \psi_V \end{bmatrix} = \psi_H \underbrace{\begin{bmatrix} 1 \\ 0 \end{bmatrix}}_{|H\rangle} + \psi_V \underbrace{\begin{bmatrix} 0 \\ 1 \end{bmatrix}}_{|V\rangle} = \psi_H |H\rangle + \psi_H |V\rangle, \tag{3}$$

wherein $\psi_H = E_H/\sqrt{I}$ ($\psi_V = E_V/\sqrt{I}$), while $|H\rangle = \begin{bmatrix} 1 & 0 \end{bmatrix}^T$ and $|V\rangle = \begin{bmatrix} 0 & 1 \end{bmatrix}^T$ represent horizontal and vertical polarization states, respectively (that are clearly orthogonal). The normalization condition is obviously satisfied:

$$|\psi_H|^2 + |\psi_V|^2 = \frac{|E_{H0}|^2 + |E_{V0}|^2}{I} = 1. \tag{4}$$

In Dirac notation, with each column-vector ("ket") $|\ \psi\rangle$, defined by (3), we associate a row-vector ("bra") $\langle\psi|$ as follows:

$$\langle\psi| = \begin{bmatrix} \psi_x^* & \psi_y^* \end{bmatrix}. \tag{5}$$

The *dot (scalar) product* of ket $|\ \phi\rangle$ bra $\langle\psi|$ is defined by the following "bracket" operation:

$$\langle\phi|\psi\rangle = \phi_x^*\psi_x + \phi_y^*\psi_y = \langle\psi|\phi\rangle^*. \tag{6}$$

Using this notation, the right- and left-circular polarization states, denoted respectively as $|R\rangle$ and $|L\rangle$, can be represented by:

$$\begin{aligned} |R\rangle &= \frac{1}{\sqrt{2}}\begin{bmatrix} 1 \\ j \end{bmatrix} = \frac{1}{\sqrt{2}}|H\rangle + \frac{j}{\sqrt{2}}|V\rangle, \\ |L\rangle &= \frac{1}{\sqrt{2}}\begin{bmatrix} 1 \\ -j \end{bmatrix} = \frac{1}{\sqrt{2}}|H\rangle - \frac{j}{\sqrt{2}}|V\rangle, \end{aligned} \tag{7}$$

which are clearly orthogonal as $\langle R|L\rangle = 0$.

The action of any polarizing element on a polarization state can be described by the *Jones operator (matrix)* J performing the action on the input state $|\psi\rangle$ by [35]:

$$|\psi_{\text{out}}\rangle = J|\psi\rangle = \begin{bmatrix} J_{HH} & J_{HV} \\ J_{VH} & J_{VV} \end{bmatrix} |\psi\rangle. \tag{8}$$

The *linear polarizer* changes the amplitude of polarization vector (state), and can be characterized by the absorption coefficients along H-axis and V-axis, denoted as a_H and a_V, respectively as follows:

$$J_{\text{polarizer}} = \begin{bmatrix} a_H & 0 \\ 0 & a_V \end{bmatrix};\ \ 0 \leqslant a_i \leqslant 1,\ \ i \in \{H,\ V\}. \tag{9}$$

The *wave plates* (also known as the retarders or the phase shifters) are polarizing devices introducing the phase shift $\phi/2$ along H-axis and the phase shift $-\phi/2$ along V-axis, and the corresponding Jones matrix is described by:

$$J_{\text{wave plate}} = \begin{bmatrix} e^{j\phi/2} & 0 \\ 0 & e^{-j\phi/2} \end{bmatrix} = e^{j\phi/2}\begin{bmatrix} 1 & 0 \\ 0 & e^{-j\phi} \end{bmatrix}. \tag{10}$$

Two popular wave plates are *quarter-wave plate*(QWP), for which ϕ=$\pi/2$, and *half-wave plate*(HWP), for which

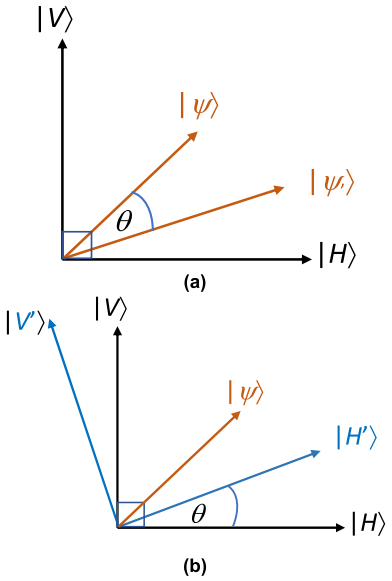

FIGURE 1. Illustrating the transformation of the polarization basis: (a) the rotation of the state vector, (b) the rotation of a coordinate system.

$\phi{=}\pi$, while the corresponding Jones matrices describing their actions are given respectively by:

$$J_{\text{QWP}} = \begin{bmatrix} 1 & 0 \\ 0 & -j \end{bmatrix}, \; J_{\text{HWP}} = \begin{bmatrix} 1 & 0 \\ 0 & -1 \end{bmatrix}. \tag{11}$$

To illustrate, when the input state to the QWP is linear $\pm 45^o$state, denoted as $|\pm 45^o\rangle{=}[\,1 \pm 1]^{\text{T}}/\sqrt{2}$, at the output it gets converted to the left-/right-circular polarization state as follows:

$$J_{\text{QWP}} \left|\pm 45^{\circ}\right\rangle = \frac{1}{\sqrt{2}} \begin{bmatrix} 1 & 0 \\ 0 & -j \end{bmatrix} \begin{bmatrix} 1 \\ \pm 1 \end{bmatrix} = \frac{1}{\sqrt{2}} \begin{bmatrix} 1 \\ \mp j \end{bmatrix}. \tag{12}$$

The third relevant polarizing element is the *rotator*, whose action is illustrated in Fig. 1, wherein the polarization state $|\psi\rangle$ is rotated for θin a clockwise direction, which is equivalent to the rotation of a given coordinate system in the opposite (counterclockwise) direction for the same angle θ, as shown in Fig. 1(b). The polarization state $|\psi\rangle$ can be represented in original the $\{|H\rangle,|V\rangle\}$ basis by:

$$|\psi\rangle = |H\rangle \langle H|\psi\rangle + |V\rangle \langle V|\psi\rangle . \tag{13}$$

From (13), we notice that the following is valid:

$$|H\rangle \langle H| + |V\rangle \langle V| = \boldsymbol{I}_2, \tag{14}$$

where $\boldsymbol{I}_2$ is 2×2 identity matrix, which is known as the *completeness relationship* in the quantum mechanics. However, our polarization states are classical, wherein each polarization state is composed of large number of photons having the same polarization. By multiplying (13) by $\langle H'|$ and $\langle V'|$ from the left side we obtain:

$$\left|\psi'\right\rangle = \begin{bmatrix} \langle x'|\psi\rangle \\ \langle y'|\psi\rangle \end{bmatrix} = \begin{bmatrix} \langle x'|x\rangle & \langle x'|y\rangle \\ \langle y'|x\rangle & \langle y'|y\rangle \end{bmatrix} \begin{bmatrix} \langle x|\psi\rangle \\ \langle y|\psi\rangle \end{bmatrix}$$

$$= \underbrace{\begin{bmatrix} \cos\theta & \sin\theta \\ -\sin\theta & \cos\theta \end{bmatrix}}_{J(\theta)} \begin{bmatrix} \langle x|\psi\rangle \\ \langle y|\psi\rangle \end{bmatrix}$$

$$= J(\theta)\,|\psi\rangle , \tag{15}$$

where $J(\theta)$ is the Jones rotation matrix, which is simultaneously the basis transformation matrix.

By using these three polarizing elements we can obtain an arbitrary elliptic polarization state starting from the coherent state. Therefore, we have already introduced the concepts relevant in quantum mechanics such as the superposition principle (13), the completeness relationship (14), and the change of basis (15), while manipulating the classical polarization states.

Now we describe how to entangle classical coherent states [1], [25]. The coherent state $|\alpha\rangle$, where α is a complex number [that is $\alpha{=}|\alpha|\exp(\text{j}\varphi)$], can be represented in terms of number (Fock) states $|n\rangle$ as follows [17], [23]:

$$|\alpha\rangle = \exp\left[-|\alpha|^2/2\right] \sum_{n=0}^{+\infty} (n!)^{-1/2} \alpha^n |n\rangle , \; \alpha = |\alpha| e^{j\varphi} \tag{16}$$

One of the important properties of coherent states is that the coherent state is an eigen vector of the annihilation operator $\hat{a}$ (decreasing the degree of excitation for 1), that is:

$$\hat{a}\,|\alpha\rangle = \alpha\,|\alpha\rangle . \tag{17}$$

The coherent state can also be represented as a displaced vacuum state by:

$$\hat{D}(\alpha)\,|0\rangle = |\alpha\rangle , \; \hat{D}(\alpha) = \exp\left(\alpha\hat{a}^{\dagger} - \alpha^{*}\hat{a}\right), \tag{18}$$

where $\hat{D}(\alpha)$ is the displacement operator. Based on Fig. 2 of ref. [25], we can entangle two continuous variable (CV) states with the help of two periodically polled lithium niobate (PPLN) crystals or waveguides serving the role of single-photon addition modules. The corresponding circuit to entangle two coherent states $|\alpha\rangle$ and $|\beta\rangle$, based on Figs. 2 and 9 of ref. [25], is provided in Fig. 2, where we use $\hat{a}^{\dagger}$ to denote the creation operator (increasing the degree of excitation for 1). The same pump laser is used to operate both PPLN modules, whose power is split by the power splitter. Each pump photon in either PPLN modules generates entangled signal and idler photons. The idler modes are interacted on the beam splitter. If the input states where CV states, after the beam splitter we will not be able to identify if the click on single photon detector 1 (SPD1)/SPD2 originating from upper or lower PPLN module, thus making the input CV states entangled [25]:

$$|\psi_{\text{out}}\rangle = \mathcal{X}^{-1/2} \left(\hat{a}^{\dagger}|\alpha\rangle_1|\beta\rangle_2 + e^{j\phi}|\alpha\rangle_1\hat{b}^{\dagger}|\beta\rangle_2\right), \tag{19}$$

where $\mathcal{X}$ is the normalization factor. However, this is not always true when the input states are coherent states. By using the symmetry properties of the displacement operator we

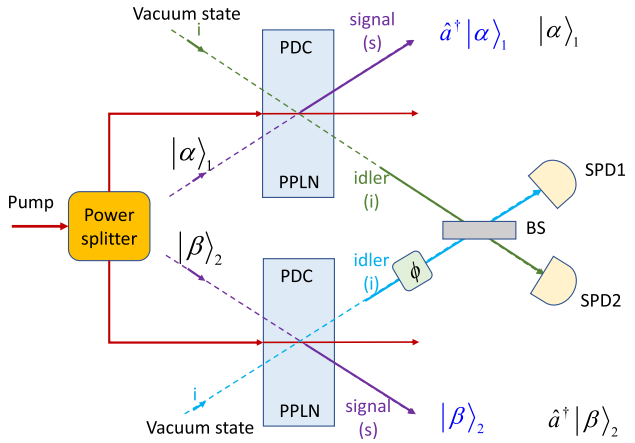

FIGURE 2. LiNbO $_3$ technology-based circuit to entangle two coherent states. PDC: parametric down conversion, PPLN: periodically poled lithium niobate crystal (or waveguide), BS: beam splitter, SPD: single-photon detector.

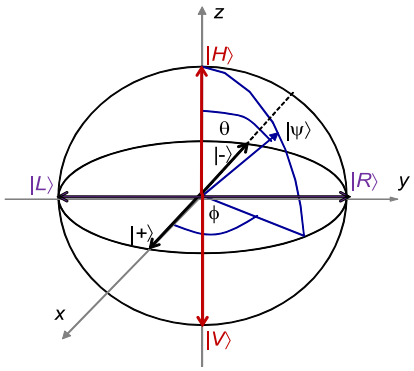

FIGURE 3. The Poincaré sphere representation of the classical polarization states.

arrive to the following relationship $\hat{a}^\dagger \hat{D}(\alpha) = \hat{D}(\alpha)(\hat{a}^\dagger + \alpha^*)$, which allows us to re-write the (19) as follows:

$$|\psi_{\text{out}}\rangle = \mathcal{X}^{-1/2}\hat{D}_1(\alpha)\hat{D}_2(\beta)\left(|1\rangle_1|0\rangle_2 + e^{j\phi}|0\rangle_1|1\rangle_2\right) \mathcal{X}^{-1/2}\alpha^*\left(1+e^{j\phi}\right)|\alpha\rangle_1|\beta\rangle_2, \quad (20)$$

wherein the first term is an entangled state, while the second term is a separable state. By setting the phase shift on phase trimmer (see Fig. 2) to $\phi{=}\pi$ rad, the separable term is removed, and we have been able to entangle two coherent states:

$$|\psi_{\text{out}}\rangle_{\phi=0} = \mathcal{X}^{-1/2}\hat{D}_1(\alpha)\hat{D}_2(\beta)(|1\rangle_1|0\rangle_2 + |0\rangle_1|1\rangle_2). \quad (21)$$

Based on the above we conclude that linear superposition and entanglement are also applicable to the classical states and are not exclusive to the quantum mechanics, which is contrary to the common belief [5], [10], [20], [24].

Before concluding this section, it is convenient to introduce the *Poincaré sphere* representation of the classical polarization state given by (3), which is in quantum mechanics

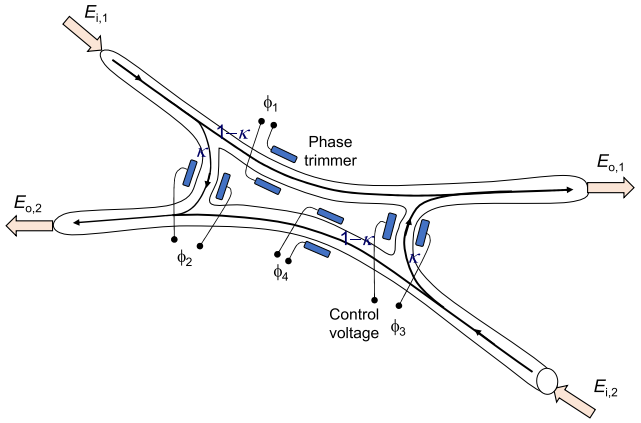

FIGURE 4. The optical hybrid suitable for both coherent detector and classical single-qubit gates analogs implementations.

known as the Bloch sphere. The coefficients ψ_{H} and ψ_{V} are complex numbers, and therefore can be represented as $\psi_H = |\psi_H|\exp(j\phi_H)$, $\psi_V = |\psi_V|\exp(j\phi_V)$, so that we can re-write (3) as follows:

$$|\psi\rangle = e^{j\phi_H}\left(|\psi_H||H\rangle + e^{j\overbrace{(\phi_V-\phi_H)}^{\phi}}|\psi_V||V\rangle\right),\ \phi = \phi_V - \phi_H, \quad (22)$$

and by parametrizing the magnitudes of complex numbers by $|\psi_H| = \cos(\theta/2)$, $|\psi_V| = \sin(\theta/2)$ and ignoring the global phase shift we arrive at the following representation:

$$|\psi\rangle = \cos\left(\frac{\theta}{2}\right)|H\rangle + e^{j\phi}\sin\left(\frac{\theta}{2}\right)|V\rangle = \begin{bmatrix}\cos\left(\frac{\theta}{2}\right)\\ e^{j\phi}\sin\left(\frac{\theta}{2}\right)\end{bmatrix}, \quad (23)$$

where $\phi \in [0, 2\pi]$ and $\theta \in [0, \pi]$, which is illustrated in Fig. 3.

The north and south poles correspond to the computational basis $\{|H\rangle,|V\rangle\}$. The diagonal basis is defined by two-unit vectors placed along the x-axis $\{|+\rangle,|-\rangle\}$, while the circular basis by two-unit vectors placed along the y-axis $\{|R\rangle, |L\rangle\}$.

III. CLASSICAL SINGLE-QUBIT GATES ANALOGS IMPLEMENTED IN INTEGRATED OPTICS

The 2×2 optical hybrid has been considered in our previous publications in the context of coherent detection to mix the received signal and local oscillator (LO) laser signal [35] as well as in the context of single-qubit gates implementation in integrated optics [11], [12], [15], [16], [17]. Here we consider a particular version of 2×2 optical hybrid with four phase trimmers, provided in Fig. 4, suitable for manipulation of the classical polarization states. This device is composed of two input ports, two input Y-junctions, two output Y-junctions, two output ports, and four phase trimmers. Based on Fig. 4 we conclude that the output electric fields $E_{o,1}$ and $E_{o,2}$ are

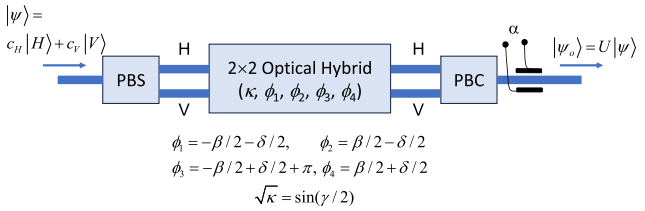

FIGURE 5. The 2×2 optical classical hybrid-based single-qubit gate analog suitable for implementation in the integrated optics.

related to the input electric fields $E_{i,1}$ and $E_{i,2}$ as follows:

$$E_{o,1} = \sqrt{1-\kappa}e^{j\phi_1}E_{i,1} + \sqrt{\kappa}e^{j\phi_3}E_{i,2},$$
$$E_{o,2} = \sqrt{\kappa}e^{j\phi_2}E_{i,1} + \sqrt{1-\kappa}e^{j\phi_4}E_{i,2}. \tag{24}$$

The corresponding matrix representation is given by:

$$\boldsymbol{E}_o = \begin{bmatrix} E_{o,1} \\ E_{o,2} \end{bmatrix} = \underbrace{\begin{bmatrix} \sqrt{1-\kappa}e^{j\phi_1} & \sqrt{\kappa}e^{j\phi_3} \\ \sqrt{\kappa}e^{j\phi_2} & \sqrt{1-\kappa}e^{j\phi_4} \end{bmatrix}}_{S} \underbrace{\begin{bmatrix} E_{i,1} \\ E_{i,2} \end{bmatrix}}_{E_i} = \boldsymbol{S}\boldsymbol{E}_i, \tag{25}$$

where $\boldsymbol{S}$ is the scattering matrix defined by:

$$\boldsymbol{S} = \begin{bmatrix} \sqrt{1-\kappa}e^{j\phi_1} & \sqrt{\kappa}e^{j\phi_3} \\ \sqrt{\kappa}e^{j\phi_2} & \sqrt{1-\kappa}e^{j\phi_4} \end{bmatrix}, \tag{26}$$

and κ is the power splitting ratio of the corresponding Y-junction.

For instance, by setting $\phi_1 = \phi_2 = \phi_3 = 0$, $\phi_4 = \pi$, $\kappa = 1/2$ the $\boldsymbol{S}$-matrix becomes the Hadamard matrix:

$$\boldsymbol{H} = \frac{1}{\sqrt{2}}\begin{bmatrix} 1 & 1 \\ 1 & -1 \end{bmatrix}. \tag{27}$$

By placing the 2×2 optical hybrid between the polarization beam splitter (PBS) and polarization beam combiner (PBC), we obtain the circuit shown in Fig. 5, which is suitable to perform arbitrary single-qubit analog operation on a given classical polarization state.

By parametrizing the power splitting ratio by $\sqrt{\kappa} = \sin(\gamma/2)$ and setting the phase shifts as follows:

$$\phi_1 = -\beta/2 - \delta/2, \quad \phi_2 = \beta/2 - \delta/2$$
$$\phi_3 = -\beta/2 + \delta/2 + \pi, \ \phi_4 = \beta/2 + \delta/2 \tag{28}$$

the unitary matrix connecting the output and input classical polarization states is given by:

$$\boldsymbol{U} = e^{j\alpha}\begin{bmatrix} \cos(\gamma/2)\,e^{j(-\beta/2-\delta/2)} & -\sin(\gamma/2)\,e^{j(-\beta/2+\delta/2)} \\ \sin(\gamma/2)\,e^{j(\beta/2-\delta/2)} & \cos(\gamma/2)\,e^{j(\beta/2+\delta/2)} \end{bmatrix}, \tag{29}$$

which is commonly referred to as the *Y-Z decomposition theorem* in QIP literature [5]. With this representation in mind, we can represent an arbitrary single-qubit gate analog. By selecting $\alpha=\pi/2$, $\beta=0$, $\gamma=\pi/2$, and $\delta=\pi$ the $U-$gate reduces down to the Hadamard gate (27).

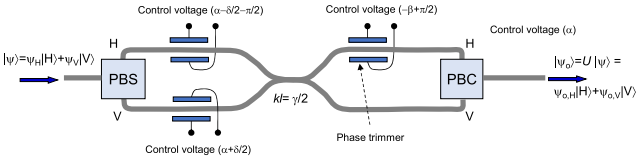

FIGURE 6. The directional coupler-based implementation of arbitrary single-qubit gate analog employing the Y-Z decomposition theorem.

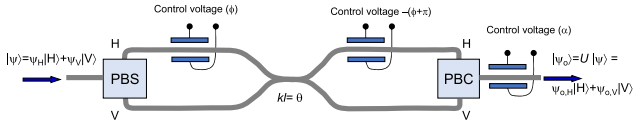

FIGURE 7. The directional coupler-based implementation of arbitrary single-qubit gate analog employing the Barenco-like gate.

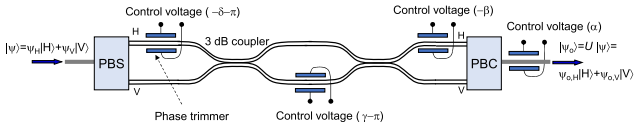

FIGURE 8. The Mach-Zehnder interferometer-based implementation of arbitrary single-qubit gate analog employing the Y-Z decomposition theorem.

The Pauli X-, Y-, and Z-gates can be implemented as follows. By selecting $\alpha=\pi/2$, $\beta=-\pi$, $\gamma=\pi$, and $\delta=0$ the $U-$gate reduces to the Pauli-X gate:

$$\boldsymbol{X} = \begin{bmatrix} 0 & 1 \\ 1 & 0 \end{bmatrix}. \tag{30.1}$$

By selecting $\alpha=\pi/2$, $\beta=0$, $\gamma=\pi$, and $\delta=0$ arrive at the Pauli-Y gate:

$$\boldsymbol{Y} = \begin{bmatrix} 0 & -j \\ j & 0 \end{bmatrix}. \tag{30.2}$$

By selecting $\alpha=\pi/2$, $\beta=\pi$, $\gamma=2\pi$, and $\delta=0$ the $U-$ gate reduces down to the Pauli-Z gate:

$$\boldsymbol{Z} = \begin{bmatrix} 1 & 0 \\ 0 & -1 \end{bmatrix}. \tag{30.3}$$

Further, by setting $\alpha=\pi/8$, $\beta=\pi/4$, $\gamma=2\pi$, and $\delta=0$ rad we obtain the $\pi/8-$gate:

$$\boldsymbol{T} = \begin{bmatrix} 1 & 0 \\ 0 & e^{j\pi/4} \end{bmatrix}. \tag{31}$$

Finally, by selecting $\alpha=\pi/4$, $\beta=\pi/2$, $\gamma=2\pi$, and $\delta=0$ rad the $U-$ gate becomes the phase-gate:

$$\boldsymbol{P} = \begin{bmatrix} 1 & 0 \\ 0 & j \end{bmatrix}. \tag{32}$$

The scattering matrix of directional coupler, used in Figs. 6 and 7, is given by [35]:

$$\boldsymbol{S} = \begin{bmatrix} \cos(kL) & j\sin(kL) \\ j\sin(kL) & \cos(kL) \end{bmatrix}, \tag{33}$$

where k is the coupling coefficient and L is the coupling region length. By selecting the coupling phase shift to be

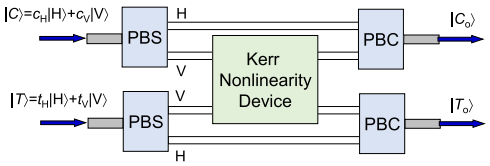

FIGURE 9. The integrated optics implementation of the controlled-phase gate analog. The Kerr nonlinearity device could be either HNLF or PPLN waveguide/crystal.

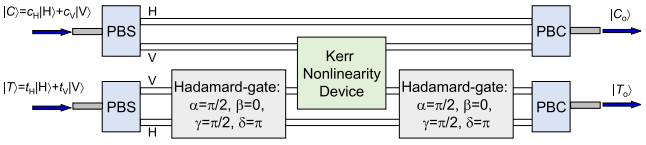

FIGURE 10. The integrated optics implementation of the classical CNOT gate analog. The Kerr nonlinearity device could be either HNLF or PPLN waveguide/crystal.

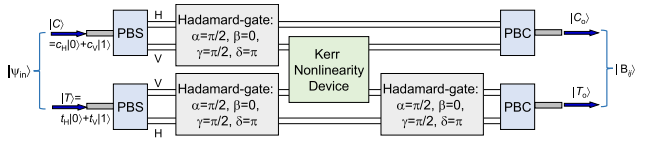

FIGURE 11. The integrated optics implementation of the classical generic Bell states preparation circuit analog. The Kerr nonlinearity device could be either HNLF or PPLN waveguide/crystal.

$kL=\gamma/2$, and by selecting the phase shifts on three phase trimers as indicated in Fig. 6, the overall scattering matrix is identical to that given by (29). Therefore, this device represents an alternative single-qubit gate analog implementation. Another version of the single-qubit gate analog is provided in Fig. 7, and it is derived from the Barenco theorem, claiming the following two-qubit gate is universal [36]:

$$\boldsymbol{A}(\phi,\alpha,\theta)=\begin{bmatrix}\boldsymbol{I}_2 & \\ & \boldsymbol{U}_B\end{bmatrix},$$
$$\boldsymbol{U}_B=\begin{bmatrix}e^{j\alpha}\cos\theta & -je^{j(\alpha+\phi)}\sin\theta\\ -je^{j(\alpha-\phi)}\sin\theta & e^{j\alpha}\cos\theta\end{bmatrix} \quad (34)$$

By selecting the coupling phase shift to be $kL=\theta$, and by selecting the phase shifts on two phase trimers as indicated in Fig. 7, the overall scattering matrix is identical to that given by $\boldsymbol{U}_B$−matrix in (34).

Finally, by using the Mach-Zehnder interferometer-based circuit provided in Fig. 8, and by selecting the phase shifts as specified in the Figure, we obtain the overall scattering matrix given by (29).

IV. CLASSICAL CONTROLLED-PHASE AND CNOT GATES ANALOGS IMPLEMENTED IN INTEGRATED OPTICS

The Barenco gate, introduced by the (34) represents the universal quantum gate. The three-qubit Deutsch gate, introduced in [37], also represents the universal quantum gate. Another popular universal set of gates is $\{H, P, T, CNOT\}$ [38].We have already described how to implement the H, P, and Tgates in the previous section, what remains is to describe how to implement the classical CNOT-gate analog. Given that $\boldsymbol{T}^2=\boldsymbol{P}$, and that CNOT gate classical analog can be expressed in terms of controlled-phase gate

$$C(Z)=\begin{bmatrix}I_2 & 0\\ 0 & Z\end{bmatrix} \text{ by:}$$
$$CNOT\,|C\rangle\,|T\rangle=|C\rangle\otimes X^C\,|T\rangle=|C\rangle\otimes(HZX)^C\,|T\rangle$$
$$=I\otimes H\cdot C(Z)\cdot I\otimes H\,|C\rangle\,|T\rangle\,, \quad (35)$$

we can reduce the set of universal quantum gates down to $\{H, T, C(Z)\}$. The photonic implementation of the C(Z) gate in integrated optics is illustrated in Fig. 9, where we employed the Kerr nonlinear effect [35] to introduce the nonlinear phase shift of π rad only between vertically polarized states so that the action of the gate can be described by:

$$C(Z)\,|H\rangle\,|H\rangle=|H\rangle\,|H\rangle\,,\ C(Z)\,|H\rangle\,|V\rangle=|H\rangle\,|V\rangle\,,$$
$$C(Z)\,|V\rangle\,|H\rangle=|V\rangle\,|H\rangle\,,\ C(Z)\,|V\rangle\,|V\rangle=-|V\rangle\,|V\rangle\,. \quad (36)$$

Namely, for sufficiently high light intensity the refractive index of nonlinear optical medium, such as optical fiber, is not only function of frequency ω, but also function of intensity of the light beam Ithat propagates through the nonlinear medium, that is we can write $n(\omega,I)=n(\omega)+n_2I$, where n_2 is the Kerr coefficient. The cross-phase modulation (XPM) will introduce the nonlinear phase shift to the target polarization state, denoted by $\Delta\Phi_T$, as follows [35]:

$$\Delta\Phi_T=2\Gamma P_C\frac{1-e^{-aL}}{L},\ \Gamma=\frac{2\pi n_2}{\lambda A_{eff}}, \quad (37)$$

where Γ is the nonlinear coefficient, A_{eff} is the effective cross-sectional area of the fiber, a is the attenuation coefficient, and P_C is the power in the control $|C\rangle$ polarization state. By properly adjusting the power P_C we can introduce π phase-shift. Given that the typical values of the nonlinear coefficient for standard SMF is small and range from 0.9-2.75 $W^{-1}km^{-1}$ [35], the highly nonlinear fiber (HNLF) can be used for this purpose. Introducing the π rad XPM phase shift is extremely difficult on a single-photon level [9], [17]; however, it is straightforward to do so on a classical level with the help of HNLFs. Unfortunately, the HNLF is not compatible with integrated optics. Alternatively, the HNLF can be replaced by the trype-0 PPLN waveguide, where the nonlinear conversion efficiency is very efficient for the vertical polarization states, and the overall circuit is suitable for implementation in the lithium niobate (LN) technology. Such PPLN waveguides are commercially available [39], and have been routinely used in our recent experiments to generate bright entangled photons for distribution of entanglement over atmospheric turbulence channels [40] and in entanglement assisted communication demonstrations over turbulent free-space optical links [41]. Based on (36), to implement the CNOT gate analog, we need to insert two Hadamard gates in the target polarization state, one before and one after the C(Z)-operation, which is illustrated in Fig. 10.

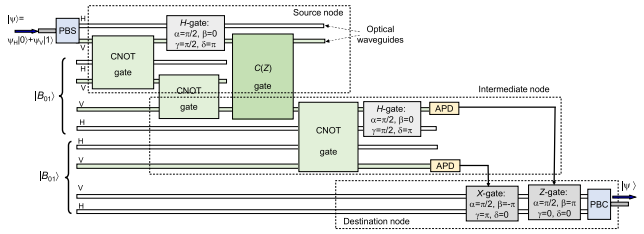

FIGURE 12. The integrated optics implementation of the classical quantum relay analog. The Kerr nonlinearity device could be either HNLF or PPLN waveguide/crystal. APD: avalanche photodiode.

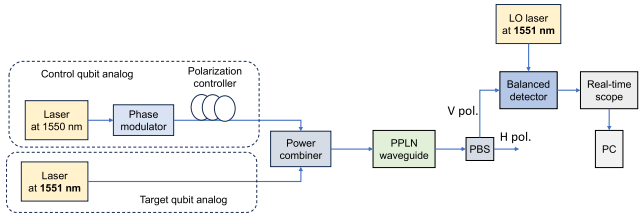

FIGURE 13. The experimental setup to demonstrate the controlled-phase operation on classical qubit analogs. PBS: polarization beam splitter, PC: personal computer.

Now we are in a position to describe an alternative way to entangle two classical polarization states, with the help of the Bell state preparation circuit, shown in Fig. 11. After applying the Hadamard gates on both control and target qubits, we apply the CNOT-gate followed by the Hadamard gate on target qubit so that the output polarization state becomes:

$$\left|B_{ij}\right\rangle = 2^{-1/2}\begin{bmatrix} c_H t_H + c_V t_V \\ c_H t_V + c_V t_V \\ c_H t_V - c_V t_V \\ c_H t_H - c_V t_H \end{bmatrix}. \tag{38}$$

Compared to the implementation from Fig. 2 only one PPLN waveguide is needed. To illustrate, by setting $c_H = 1,\ c_V = 0$ and $t_H = 0,\ t_V = 1$, we obtain the following Bell state:

$$|B_{01}\rangle = 2^{-1/2}\left[H\ V\ V\ H\right] = 2^{-1/2}\left(|H\rangle|V\rangle + |V\rangle|H\rangle\right). \tag{39}$$

By using the proposed classical single-qubit and two-qubit analogs, we can implement the quantum relay analog in integrated optics as shown in Fig. 12. The CNOT and C(Z) gates are applied between the highlighted (in green) vertical polarization basis states. We perform the measurements only at intermediate node with the help of two avalanche photodiodes (APDs) and when the vertical polarization state is detected we conditionally execute Pauli X- and Z-gates on the bottom polarization state. Clearly, the complexity of this approach is high. The better strategy will be to employ the entanglement swapping and teleportation concepts by the photon addition as we described in [25]. Corresponding quantum implementation in integrated optics is only possible as a probabilistic device [7] (performing a desired function with a certain probability), and the verification of designed function is needed, thus increasing complexity significantly.

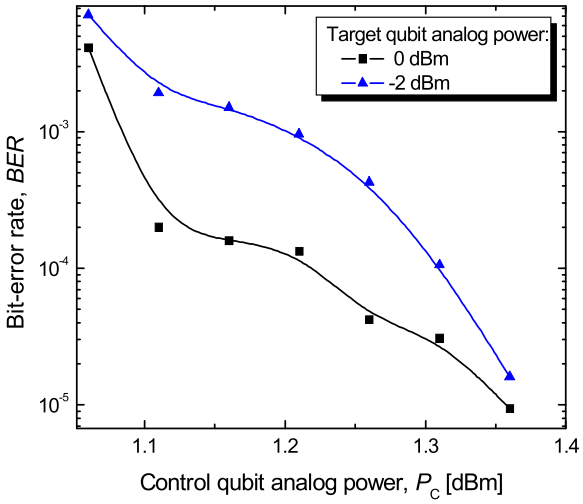

FIGURE 14. The measured BERs on vertical polarizations of target coherent sates (at 1551 nm).

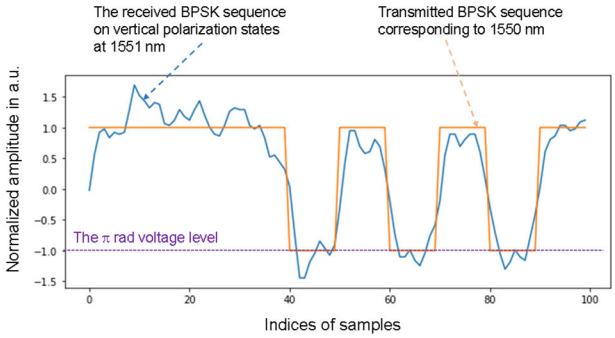

FIGURE 15. The portion of BPSK sequence received on vertical polarization states at 1551 nm. The control qubit analog is operated at 1550 nm.

To illustrate the high-potential of the proposed concept, we performed the classical controlled-phase quantum qubit analog demonstration, with experimental setup provided in Fig. 13.

The laser operated at 1550 nm generates the classical states that serve the role of the control qubit, while the bottom laser generates the states at 1551 nm that serve the role of the target qubit. To demonstrate the controlled-phase gate analog operation from Fig. 9, we need to demonstrate that control qubit coherent states can introduce the phase shift of π rad to the vertical polarization states of the target qubit analog. To do so we impose the BPSK modulation at 10 Gb/s on the control coherent states, while the target coherent states are unmodulated. We then combine the control and target coherent states by the beam combiner and conduct the cross-phase modulation (XPM) interaction of control and target coherent states by the PPLN waveguide. At the output of PPLN waveguide we separate horizontal (H) and vertical (V) polarization states by the polarization beam splitter (PBS) and perform the coherent balanced detection on vertical photons related to the target coherent states at 1551 nm. To do so we mix the local oscillator (LO) laser signal at 1551 nm with the vertical

FIGURE 16. The portion of the target qubit analog waveform recorded on real-time scope (corresponding to 1551 nm wavelength).

photons on optical hybrid (not shown in Figure) followed by the homodyne balanced detector. The detected signal is sampled by the real-time scope and sampled RF signal waveform is transferred to the personal computer (PC), where we re-sample the waveform and calculate bit log-likelihood ratios (LLRs), which are used to make decisions and determine the bit-error rates (BERs). The corresponding BER related to the target coherent state are provided in Fig. 14. The input power to the power combiner, the control power P_C, was varied, while the input power of the target coherent states was used as the parameter. For the control qubit analog powers higher than 1.4 dBm, the measured BER was zero, indicating that the BPSK get transferred completely from the control coherent states to the target coherent states, which demonstrates that the circuit from Fig. 9 indeed operates as the controlled-phase analog.

For illustrative purposes, we provide in Fig. 15 the portion of the BPSK sequence received on the vertical polarization states at 1551 nm.

The π rad voltage level is clearly indicated. Therefore, by using the XPM we were able to introduce the π rad phase shift on vertical polarization states at 1551 nm, while the control qubit analog was operated at 1550 nm thus demonstrating the controlled-phase operation. Finally, in Fig. 16, we provide the portion of the waveform record on the real-time scope corresponding to the 1551 nm target qubit analog, confirming that the sequence transferred from the control to target qubit analog is error free.

V. OPTICAL ORBITAL ANGULAR MOMENTUM GATES ANALOGS

In our papers [18] and [19] we have introduced the photon angular momentum states by combining polarization and orbital angular momentum (OAM) states, and proposed corresponding gates suitable for universal quantum computing and quantum communication applications. In this section, we provide the corresponding classical quantum gates' analogs. The OAM modes have been intensively studied for various classical communication applications, including OAM multiplexing and OAM modulations [35], [42], [43], [44], [45], [46], [47], [48], [49]. The OAM degree-of-freedom is associated with the azimuthal phase dependence of the complex electric field [35]. Among various vortex optical beams carrying the OAM, the Laguerre-Gauss (LG) vortex beams/modes are very popular and the electric field of an LG beam traveling along the z-axis can be represented in cylindrical coordinates (r,ϕ,z) (r: the radial distance from propagation axis, ϕ: the azimuthal angle, z: the propagation distance) as follows [35], [42], [45]:

$$u_{m,p}(r,\phi,z) = \sqrt{\frac{2p!}{\pi\,(p+|m|)!}}\frac{1}{w(z)}\left[\frac{r\sqrt{2}}{w(z)}\right]^{|m|} L_p^m\left(\frac{2r^2}{w^2(z)}\right) \times e^{-\frac{r^2}{w^2(z)}} e^{-\frac{jkr^2z}{2\left(z^2+z_R^2\right)}} e^{j(2p+|m|+1)\tan^{-1}\frac{z}{z_R}} e^{-jm\phi}, \tag{40}$$

where $w(z) = w_0\sqrt{1+(z/z_R)^2}$ (w_0 denotes the zero-order Gaussian radius at the waist), $z_R = \pi w_0^2/\lambda$ is the Rayleigh range (λ denotes the wavelength), $k{=}2\pi/\lambda$ is the wave number, and $L_p^m(\cdot)$ is the associated Laguerre polynomial, with p and m being the radial and angular mode numbers, respectively. It can be seen from (40) that the mth mode of the LG beam has the azimuthal angular dependence of the type $\exp(-jm\phi)$, where m is the azimuthal mode index. In free space, for $m{=}0$, $u(r,\phi,z)$ get reduced down to a zero-order Gaussian beam commonly referred to as the TEM_{00} mode. For $p{=}0$, $L_p^m(\cdot){=}1$ for values of azimuthal indices m, so that the intensity of an LG mode can be placed on a ring of radius proportional to $|m|^{1/2}$. It can be shown that for fixed p, the following principle of orthogonality is satisfied [35], [45]:

$$\langle u_{m,p}|u_{n,p}\rangle = \int u_{m,p}^*(r,\phi,z)\,u_{n,p}(r,\phi,z)\,rdrd\phi = \begin{cases} \int |u_{m,p}|^2 rdrd\phi, & n=m \\ 0, & n\neq m \end{cases} \tag{41}$$

Clearly, different OAM states corresponding to a fixed radial index p are orthogonal among each other, and as such they can be used as the basis functions for either OAM modulation or OAM multiplexing. The OAM modes can easily be generated by the computer-generated holograms (CGHs) [43], [44], [45]. The Bessel modes also belong to the class of OAM modes, and they are obtained as solutions of the wave equation in a step-index multi-mode fiber (MMF) of core radius b, with corresponding electric field z-component in cylindrical coordinates (r,ϕ,z) given by [35], [49]:

$$E_z(r,\phi,z) = AJ_m(k_r r)\,e^{-jm\phi}e^{j\beta z},\quad r\leqslant b \tag{42}$$

where $k_r = \sqrt{n_c^2k_0^2-\beta^2}$ with n_c being the refractive index of the core, $k_0{=}2\pi/\lambda$ is the free-space wave number, and β the propagation constant. We use $J_m(\cdot)$ to denote the Bessel function of the mth order. The ideal Bessel beams satisfy the relationship [50] $|E(r,\phi,z)|^2 = |E(r,\phi)|^2$ and are therefore diffraction free and as such represent excellent candidates for free-space optical (FSO) applications. It the practice, it is not trivial to generate the ideal Bessel beams and instead various approximations need to be used [51].

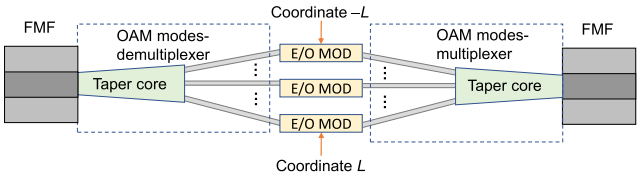

FIGURE 17. The integrated optics and FMF-based implementation of the classical single-qudit gate analog.

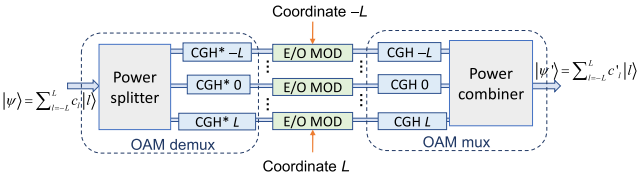

FIGURE 18. The integrated optics and CGHs-based implementation of the classical single-qudit gate analog.

Given that the OAM modes are orthogonal to each other, as shown by (41), they can be used as the basis functions $|l\rangle$ (l=−L, …, −1, 0, 1,…, L). The arbitrary spatial mode can be decomposed in terms of the basis OAM modes by:

$$|\psi\rangle = \sum_{l=-L}^{L} c_l \, |l\rangle, \tag{43}$$

assuming that the number of supported OAM modes is $2L+1$.

With this formalism at hand, given that the space here is high-dimensional, now we have to describe the OAM single-qudit and two-qudit analogs. The MMFs can be used for this purpose, given the (42); however, the MMFs support too many modes to be of practical interest. Instead, the few-mode fibers (FMFs), supporting the limited number of modes should be used as advocated in [18], [19], and [35]. The single-qudit analog, provided in Fig. 17, is similar to that proposed in our previous article [18]. The output of the FMF will contain all basis OAM modes with the same weight. In OAM modes-demultiplexer we separate the OAM basis modes, introduce the desired complex weight by the electro-optical (E/O) modulators, and recombine them by OAM modes-multiplexer before being coupled into the FMF. The CGHs-based single-qudit analog, inspired by our previous paper [19], is provided in Fig. 18. We first separate the OAM modes with corresponding complex coefficients with the help of power splitter and complex-conjugate CGHs. Each coordinate gets modified by the E/O modulators to perform a desired qudit operation. The CGHs impose the lth OAM mode (l=−L, …, 0, …, L) corresponding to the l−th coordinate, and such weighted OAM modes are combined to generate the output mode.

The generalized controlled-phase gate analog is provided in Fig. 19. The CGHs impose desired spatial modes. We use highly nonlinear FMF to interact the control $|C\rangle$ and target $|T\rangle$ qudit. Assuming that $(2L + 1)$ is a prime number, the generalized Z-gate is defined by [17], [18], [19]:

$$Z(b)\,|x\rangle = e^{j\frac{2\pi}{2L+1}b}\,|x\rangle\,, \tag{44}$$

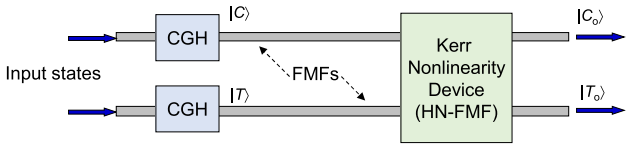

FIGURE 19. The integrated optics and FMF-based implementation of the generalized two-qudit controlled-phase gate analog.

and by adjusting the power of the control mode, we can introduce the desired nonlinear phase shift on the target qubit with the help of XPM. Instead of the HN-FMF, the PPLN waveguide/crystal can be used that now supports a desired number of higher order spatial modes.

VI. CONCLUDING REMARKS

Inspired by recent findings that the classical states can be entangled [1], [2], the CNOT gate can be implemented using the classical acoustic qubit-analog [3], and that quantum parallelism can be achieved on classical quantum computing acoustic analog [4], in this paper we propose how to implement quantum information processing analogs in integrated optics based on classical polarization and OAM states.

By using the Jones formalism we have shown that arbitrary classical polarization state can be represented as the superposition of horizontal and vertical basis polarization states. We have also shown that the quantum mechanics relevant concepts such as the superposition principle, the completeness relationship, and the change of basis are also applicable to the classical polarization states. To obtain any classical polarization state only three polarizing elements are sufficient: polarizer, wave-plate, and rotator.

We have shown that any two classical coherent states can be entangled with the help of single photon addition module, based on two PPLN waveguides.

We have further described how to implement an arbitrary single-qubit gate analog in integrated optics using any of the following three devices: 2×2 optical hybrid with four phase trimmers, directional coupler with three phase trimmers, and Mach-Zehnder interferometer with four phase trimmers. We have then described how to implement controlled-phase and CNOT gates analogs operating on classical polarization states in the lithium niobate technology. This completes the implementation of universal quantum gates analogs for classical polarization states. We have also described how to implement Bell states preparation circuit and quantum relay in the same technology. We have experimentally demonstrated the controlled-phase operation between two classical coherent states. Therefore, we have demonstrated that the classical implementation of universal quantum gates in integrated optics is possible.

The focus has been then moved to the spatial modes, and we have shown that an arbitrary classical spatial mode can be decomposed in terms of basis OAM modes. Therefore, the spatial modes can be used as the classical qudit analogs. We have described how to implement arbitrary single-qudit gate analog in either FMF or CGH technologies. We have also

described how to implement the generalized control-phase two-qudit classical analog.

This paper, therefore, represents a step forward creating a decoherence-free optical quantum information processing and computing analog, which does not rely on the fragile quantum states but rather robust classical states. Moreover, the classical states can be measured without causing the state collapse, which is unavoidable for quantum states. Given that ref. [4] has already shown that certain quantum algorithms exploiting the quantum parallelism can be implemented in classical quantum computing acoustic analog platform, the existing quantum algorithms need to be revisited for the true quantum advantages. Further, the proposed classical optical quantum computing analogs do not require delicate quantum error correction. Finally, fault tolerance is not needed in classical quantum computing analogs.

REFERENCES

[1] N. Biagi, L. S. Costanzo, M. Bellini, and A. Zavatta, "Entangling macroscopic light states by delocalized photon addition," *Phys. Rev. Lett.*, vol. 124, no. 3, Jan. 2020, Art. no. 033604.

[2] M. A. Hasan, K. Runge, and P. A. Deymier, "Experimental classical entanglement in a 16 acoustic qubit-analogue," *Sci. Rep.*, vol. 11, no. 1, p. 24248, Dec. 2021.

[3] K. Runge, M. A. Hasan, J. A. Levine, and P. A. Deymier, "Demonstration of a two-bit controlled-NOT quantum-like gate using classical acoustic qubit-analogues," *Sci. Rep.*, vol. 12, no. 1, p. 14066, Aug. 2022.

[4] P. A. Deymier, K. Runge, M. A. Hasan, T. D. Lata, J. A. Levine, and P. Cutillas, "Realizing acoustic qubit analogues with nonlinearly tunable phi-bits in externally driven coupled acoustic waveguides," *Sci. Rep.*, vol. 13, no. 1, p. 635, Jan. 2023.

[5] M. A. Neilsen and I. L. Chuang, *Quantum Computation and Quantum Information*. Cambridge, U.K.: Cambridge Univ. Press, 2000.

[6] T. C. Ralph, N. K. Langford, T. B. Bell, and A. G. White, "Linear optical controlled-NOT gate in the coincidence basis," *Phys. Rev. A, Gen. Phys.*, vol. 65, no. 6, Jun. 2002, Art. no. 062324.

[7] H. W. Li, S. Przeslak, A. O. Niskanen, J. C. F. Matthews, A. Politi, P. Shadbolt, A. Laing, M. Lobino, M. G. Thompson, and J. L. O'Brien, "Reconfigurable controlled two-qubit operation on a quantum photonic chip," *New J. Phys.*, vol. 13, no. 11, Nov. 2011, Art. no. 115009.

[8] J. Chen, J. B. Altepeter, M. Medic, K. F. Lee, B. Gokden, R. H. Hadfield, S. W. Nam, and P. Kumar, "Demonstration of a quantum controlled-NOT gate in the telecommunications band," *Phys. Rev. Lett.*, vol. 100, no. 13, Apr. 2008, Art. no. 133603.

[9] I. Fushman, D. Englund, A. Faraon, N. Stoltz, P. Petroff, and J. Vu ković, "Controlled phase shifts with a single quantum dot," *Science*, vol. 320, no. 5877, pp. 769–772, May 2008.

[10] F. Gaitan, *Quantum Error Correction and Fault Tolerant Quantum Computing*. Boca Raton, FL, USA: CRC Press, 2008.

[11] I. B. Djordjevic, "Photonic quantum dual-containing LDPC encoders and decoders," *IEEE Photon. Technol. Lett.*, vol. 21, no. 13, pp. 842–844, Jul. 1, 2009.

[12] I. B. Djordjevic, "On the photonic implementation of universal quantum gates, bell states preparation circuit, quantum relay and quantum LDPC encoders and decoders," *IEEE Photon. J.*, vol. 2, no. 1, pp. 81–91, Feb. 2010.

[13] I. B. Djordjevic, "On the photonic implementation of universal quantum gates, bell states preparation circuit and quantum LDPC encoders and decoders based on directional couplers and HNLF," *Opt. Exp.*, vol. 18, no. 8, pp. 8115–8122, Apr. 2010.

[14] I. B. Djordjevic, "Photonic entanglement-assisted quantum low-density parity-check encoders and decoders," *Opt. Lett.*, vol. 35, no. 9, pp. 1464–1466, May 2010.

[15] I. B. Djordjevic, "Photonic implementation of quantum relay and encoders/decoders for sparse-graph quantum codes based on optical hybrid," *IEEE Photon. Technol. Lett.*, vol. 22, no. 19, pp. 1449–1451, Oct. 1, 2010.

[16] I. B. Djordjevic, "Cavity quantum electrodynamics (CQED)-based quantum LDPC encoders and decoders," *IEEE Photon. J.*, vol. 3, no. 4, pp. 727–738, Aug. 2011.

[17] I. B. Djordjevic, *Quantum Information Processing, Quantum Computing, and Quantum Error Correction: An Engineering Approach*, 2nd ed. Amsterdam, The Netherlands: Elsevier, 2021.

[18] I. B. Djordjevic, "Multidimensional QKD based on combined orbital and spin angular momenta of photon," *IEEE Photon. J.*, vol. 5, no. 6, Dec. 2013, Art. no. 7600112.

[19] I. B. Djordjevic, "Integrated optics modules based proposal for quantum information processing, teleportation, QKD, and quantum error correction employing photon angular momentum," *IEEE Photon. J.*, vol. 8, no. 1, pp. 1–12, Feb. 2016.

[20] G. Cariolaro, *Quantum Communications*. Cham, Switzerland: Springer, 2015.

[21] S.-K. Liao et al., "Satellite-to-ground quantum key distribution," *Nature*, vol. 549, pp. 43–47, Aug. 2017.

[22] I. B. Djordjevic, *Physical-Layer Security and Quantum Key Distribution*. Cham, Switzerland: Springer, 2019.

[23] I. B. Djordjevic, *Quantum Communication, Quantum Networks, and Quantum Sensing*. Amsterdam, The Netherlands: Elsevier, 2022.

[24] R. van Meter, *Quantum Networking*. Hoboken, NJ, USA: Wiley, 2014.

[25] I. B. Djordjevic, "Hybrid CV-DV quantum communications and quantum networks," *IEEE Access*, vol. 10, pp. 23284–23292, 2022.

[26] Z. Zhang and Q. Zhuang, "Distributed quantum sensing," *Quantum Sci. Technol.*, vol. 6, no. 4, Oct. 2021, Art. no. 043001.

[27] *Accessing Quantum Computing*. Accessed: Mar. 1, 2024. [Online]. Available: https://www.ibm.com/quantum/pricing

[28] *Quantum Cloud Services*. Accessed: Mar. 1, 2024. [Online]. Available: https://www.rigetti.com/about-rigetti-computing

[29] *Google Quantum AI*. Accessed: Mar. 1, 2024. [Online]. Available: https://quantumai.google/

[30] R. LaRose, "Overview and comparison of gate level quantum software platforms," *Quantum*, vol. 3, p. 130, Mar. 2019.

[31] J. D. Hidary, *Quantum Computing: An Applied Approach*. Cham, Switzerland: Springer, 2019.

[32] G. Keiser, *Optical Fiber Communications*. Boston, MA, USA: McGraw-Hill, 2000.

[33] P. A. M. Dirac, *Quantum Mechanics*, 4th ed. London, U.K.: Oxford Univ. Press, 1958.

[34] J. J. Sakurai, *Modern Quantum Mechanics*. Reading, MA, USA: Addison-Wesley, 1994.

[35] I. B. Djordjevic, *Advanced Optical and Wireless Communications Systems*. Cham, Switzerland: Springer, 2018.

[36] A. Barenco, "A universal two-bit gate for quantum computation," *Proc. Roy. Soc. London. Ser. A, Math. Phys. Sci.*, vol. 449, pp. 679–683, Jun. 1995.

[37] D. Deutsch, "Quantum computational networks," *Proc. Roy. Soc. London A, Math. Phys. Sci.*, vol. 425, pp. 73–90, Sep. 1989.

[38] P. O. Boykin, T. Mor, M. Pulver, V. Roychowdhury, and F. Vatan, "On universal and fault-tolerant quantum computing: A novel basis and a new constructive proof of universality for Shor's basis," in *Proc. 40th Annu. Symp. Found. Comput. Sci.* Los Alamitos, CA, USA: IEEE Press, Oct. 1999, pp. 486–494.

[39] HC Photonics. *PPLN Mixers*. Accessed: Mar. 1, 2024. [Online]. Available: https://www.hcphotonics.com/ppln-mixers

[40] V. Nafria and I. B. Djordjevic, "Multi-wavelength entanglement distribution over turbulent free-space optical link with wavefront corrections from adaptive optics," in *Proc. 23rd Int. Conf. Transparent Opt. Netw. (ICTON)*, Bucharest, Romania, Jul. 2023, pp. 2–6.

[41] V. Nafria and I. B. Djordjevic, "Entanglement assisted communication over the free-space optical link with azimuthal phase correction for atmospheric turbulence by adaptive optics," *Opt. Exp.*, vol. 31, no. 24, p. 39906, Nov. 2023.

[42] I. B. Djordjevic and M. Arabaci, "LDPC-coded orbital angular momentum (OAM) modulation for free-space optical communication," *Opt. Exp.*, vol. 18, no. 24, pp. 24722–24728, Nov. 2010.

[43] I. B. Djordjevic and Z. Qu, "Coded orbital angular momentum modulation and multiplexing enabling ultra-high-speed free-space optical transmission," in *Optical Wireless Communications—An Emerging Technology*, M. Uysal, C. Capsoni, Z. Ghassemlooy, A. Boucouvalas, and E. G. Udvary, Eds. Cham, Switzerland: Springer, 2016, pp. 363–385.

[44] I. B. Djordjevic and Z. Qu, "Coded orbital angular momentum based free-space optical transmission," in *Wiley Encyclopedia of Electrical and Electronics Engineering*. Hoboken, NJ, USA: Wiley, Feb. 2016, doi: 10.1002/047134608X.W8291.
[45] J. A. Anguita, J. Herreros, and I. B. Djordjevic, "Coherent multimode OAM superpositions for multidimensional modulation," *IEEE Photon. J.*, vol. 6, no. 2, pp. 1–11, Apr. 2014.
[46] I. B. Djordjevic, "Multidimensional OAM-based secure high-speed wireless communications," *IEEE Access*, vol. 5, pp. 16416–16428, 2017.
[47] I. B. Djordjevic, "OAM-based hybrid free-space optical-terahertz multidimensional coded modulation and physical-layer security," *IEEE Photon. J.*, vol. 9, no. 4, pp. 1–12, Aug. 2017.
[48] T.-L. Wang, J. A. Gariano, and I. B. Djordjevic, "Employing Bessel–Gaussian beams to improve physical-layer security in free-space optical communications," *IEEE Photon. J.*, vol. 10, no. 5, pp. 1–13, Oct. 2018.
[49] I. B. Djordjevic, S. Zhang, and T. Wang, "Physical-layer security in optical communications enabled by Bessel modes," in *Proc. IEEE Photon. Conf. (IPC)*, Lake Buena Vista, FL, USA, Oct. 2017, pp. 719–720.
[50] D. McGloin and K. Dholakia, "Bessel beams: Diffraction in a new light," *Contemp. Phys.*, vol. 46, no. 1, pp. 15–28, Jan. 2005.
[51] T.-L. Wang, I. B. Djordjevic, and J. Nagel, "Laser beam propagation effects on secure key rates for satellite-to-ground discrete modulation CV-QKD," *Appl. Opt.*, vol. 58, no. 29, pp. 8061–8068, Oct. 2019.

IVAN B. DJORDJEVIC (Fellow, IEEE) received the Ph.D. degree from the University of Nis, Yugoslavia, in 1999.

He is currently a Professor in electrical and computer engineering and optical sciences with the University of Arizona; the Director of the Optical Communications Systems Laboratory (OCSL) and the Quantum Communications (QuCom) Laboratory; and the Co-Director of the Signal Processing and Coding Laboratory. He is the faculty member of the the Science and Technology Center New Frontiers of Sound supported by the NSF. Prior to joining the University of Arizona, he held appointments with the University of Bristol, University of the West of England, U.K., Tyco Telecommunications, USA, National Technical University of Athens, Greece, and State Telecommunication Company, Yugoslavia. He has authored or coauthored 11 books, more than 590 journals and conference publications, and he holds 57 U.S. patents.

Dr. Djordjevic is a fellow of Optica (formerly OSA). He serves as an Editor/Member of Editorial Board for the following journals, such as IEEE TRANSACTIONS ON COMMUNICATIONS, *Optical and Quantum Electronics*, and *Frequenz*. He was served as an Associate Editor for IEEE/Optica JOURNAL OF OPTICAL COMMUNICATIONS & NETWORKING, from 2019 to 2022. Furthermore, he was served as an Editor/Senior Editor/Area Editor for IEEE COMMUNICATIONS LETTERS, from 2012 to 2021. He was served as an Editorial Board Member/Associate Editor for *Journal of Optics* (IOP) and *Physical Communication* journal (Elsevier), from to 2016 to 2021.

VIJAY NAFRIA received the M.S. degree in ECE from the University of Arizona, in 2014, where he is currently pursuing the Ph.D. degree with the Department of Electrical and Computer Engineering. He is also doing experimental research in the fields of quantum and classical optical communications operated over turbulent terrestrial free-space optical links.